The Nucleus ***63***, *No. 2 (2026) 1-9*

https://doi.org/10.71330/thenucleus.2026.1520

www.thenucleuspak.org.pk

The Nucleus

ISSN 0029-5698 (Print)
ISSN 2306-6539 (Online)

Structural, Electronic, Magnetic, and Thermoelectric Properties of Cr-doped DPs Cs_2GeX_6 (X= Cl, Br): DFT calculations

Sultan Abbas, M. Aslam Khan*, Shanawer Niaz

Institute of Physics, Khwaja Fareed University of Engineering and Information Technology, 64200, Rahim Yar Khan, Pakistan

ABSTRACT

Physical properties of chromium-doped halide double perovskites (DPs) Cs_2GeX_6 (X= Cl, Br) are estimated with respect to the DFT-based software Wein2k. These materials can be selected for solar cells and photovoltaics owing to their non-toxicity and ecological sustainability. Density functional theory (DFT) calculations investigate the physical characteristics of halides A_2BX_6 (A=Cs; B=Ge; X=Cl, Br), both pure and Cr-doped, which can potentially be applied to thermoelectric applications. Formation conditions and tolerance factors ensure the material's structural and thermodynamic feasibility. The band gap of the material Cs_2GeCl_6 is 4.5 eV; the same for the doped one $Cs_2Ge_{0.75}Cr_{0.25}Cl_6$ is 4.1 eV; the band gap of the material Cs_2GeBr_6 is 3.0 eV, while that of the doped material $Cs_2Ge_{0.75}Cr_{0.25}Br_6$ is 2.5 eV. $Cs_2Ge_{0.75}Cr_{0.25}Cl_6$ and $Cs_2Ge_{0.75}Cr_{0.25}Br_6$ have indirect band gaps, respectively. Furthermore, when the chromium doping ratio increases, so do the equilibrium lattice parameters of Cs_2GeCl_6 and Cs_2GeBr_6. Cs_2GeCl_6: 10.32 Å, $Cs_2Ge_{0.75}Cr_{0.25}Cl_6$: 10.55 Å, and Cs_2GeBr_6: 10.65 Å, $Cs_2Ge_{0.75}Cr_{0.25}Br_6$: 10.85 Å are the calculated lattice parameters. Both compounds have the same total magnetic moment values with 25% Cr doping for $Cs_2Ge_{0.75}Cr_{0.25}Cl_6$ and $Cs_2Ge_{0.75}Cr_{0.25}Br_6$. As a result, all of the halides investigated are commonly employed in thermoelectric devices. Thermal conductivity, electrical conductivity, and the Seebeck coefficient are also used to investigate thermoelectric properties. The computed values for PF at 200 K are PF=1.90× $10^{11}W/K^2ms$ and 1.85× $10^{11}W/K^2ms$, and PF=3.98× $10^{11}W/K^2ms$ and 4.09× $10^{11}W/K^2$mat 800 K are measured for $Cs_2Ge_{0.75}Cr_{0.25}Cl_6$ and $Cs_2Ge_{0.75}Cr_{0.25}Br_6$, respectively, highlighting their importance in thermoelectric applications. The Seebeck coefficient value drops as temperature increases.

Keywords: *Cr-doping, Structural property, Electronic property, Thermoelectric property, Magnetic property, Density functional theory*

1. Introduction

The recently obtained results show that double halide perovskites can be considered as prospective materials in luminescence and photovoltaics. Despite great progress in materials science, a problem remains in accurately defining "perovskite." Therefore, we will define our concept of perovskite materials with an additional specification of "higher halides," i.e., Cl, Br, and I. It's necessary to specify distinguishing features of halide perovskites within this definition and point out crystal structures that are not regarded as perovskites despite being close to this class in terms of structural characteristics [1]. Rapid growth of world population, combined with the use of modern electronics and other technologies, leads to a constant need for energy that is hardly supplied using conventional sources. Therefore, much work has focused on improving the efficiency of various renewable technologies [2, 5], including thermoelectric devices and solar cells. To improve the performance of solar cells and other photovoltaic devices, properties of halide double perovskite materials should be optimized [6, 10]. Double halide perovskites are considered highly efficient and reliable materials in solar cells and photovoltaics [11, 12]. They exist as organic–inorganic and purely inorganic perovskites, but double perovskites are mostly produced from the inorganic composition of the mentioned compounds. Their unusual structure and physical properties make them of great interest in materials science research [13]. Initially, organic-inorganic double perovskites were used to create dye-sensitized solar cells (DSSCs), but their low efficiency made large-scale production impossible [14, 15].

Further research shows that using inorganic HDP materials can increase device efficiency and stability. For example, several investigations demonstrate the efficiency of HDP-based solar cell techniques compared to traditional silicon-based photovoltaics [16]. Other renewable energy sources can use halide double perovskites to capture heat produced by commercial electronic and mechanical equipment. The Pb-free double perovskites A_2BX_6 (where A = Cs, B = Ge, X = Cl, Br) can be considered one of the best materials for renewable energy and an alternative to hybrid halide perovskites [17]. When discussing HDP halides, adding Pb to improve device stability and efficiency seems inevitable. Lead is highly poisonous and can threaten people's health [18]. Another disadvantage of lead in this context is its instability under long-term solar irradiation. Double halide perovskites are among the most promising compounds for solar cells and similar technologies and will most likely be used to manufacture lasers, solar cells, photovoltaic absorbers, and light-emitting diodes [19]. That is why scientists strive to replace Pb with other elements, such as Ge^{2+} and $Sn^{2+,}$ which are more environmentally friendly and can improve efficiency and stability. However, these ions are unstable because they are easily oxidized [20, 21]. Replacing Pb^{2+} with Bi^{3+} and Sb^{3+} does not improve performance [22, 23]. The future of these materials may lie in bivalent [24] and heterovalent doping [25].

The formation of a direct bandgap is another commonly observed characteristic of double perovskite halides. Their properties depend on controlling the stoichiometric ratio between the constituent elements [26, 28]. Stabilizing a

*Corresponding author: greatkhan17@gmail.com

particular crystal structure through composition tuning is one clear benefit. To improve stability and effectiveness, it is necessary to increase the number of possible cation substitutions in these materials. This purpose could be achieved with the help of vacancy-ordered double perovskite halides, when half of the B-site cations from the AB_2X_6 compound are eliminated [29].

Because of the interesting magnetic ordering and tunable electronic properties of these double perovskites, some Cr-containing compositions, such as Nd_2FeCrO_6 and La_2CrCoO_6, have been reported as good candidates for spintronics [30]. Despite this progress, Cr-substituted lead-free double perovskites still lack detailed investigation, especially using a single approach to study their stability, magnetic ordering, electronic structure, thermoelectric properties, and optical properties [31]. In addition, studies that explore all these properties using a first-principles approach are relatively rare. Recent first-principles studies have shown that optical, electrical, and photovoltaic properties of double perovskites can be tuned by varying composition and engineering the electronic structure. In this regard, Zhang et al. studied the energy band gaps and electronic structures of $CsGeX_3$ (X=Cl, Br, I) materials in the visible range. Other optical properties of Cs_2SnI_6, including a 1.6 eV bandgap, were studied in terms of their applicability in photovoltaic devices [32]. Many advancements in halide double perovskite applications for solar energy harvesting have been made [33]. An extensive group of double perovskites of A_2BX_6 type was analyzed by Wang et al. in the context of their utilization in solar cells when A = Cs, Rb, Tl; B - a tetrahedral cation; X = Cl, Br, I [34]. Halide perovskites are promising materials for thermoelectric devices and photovoltaics because of their environmentally friendly compositions. Cr-doping in halide double perovskites of the general formula Cs_2GeX_6 (X = Cl, Br) was examined with the help of DFT [35].

2. Methodologies

DFT is a widely used method for computing the structures and optical and electrical properties of crystals. We used Wien2k [36] to calculate the physical characteristics of doped and undoped compositions. Ground-state structural properties were determined by optimization and relaxation of the arrangement of the double perovskite's unit cell structure. We calculated optical and electrical properties using the optimized structural parameters. In this work, we solved the Kohn-Sham equations using first-principles methods with the Wien2k program and its related simulation packages. Geometry optimization has been performed with GGA-PBE [37], and electronic structure calculations have been performed with the well-known modified Becke-Johnson (mBJ) exchange potential [38], which is known to produce much better predictions of band gaps of semiconductors and insulators than conventional GGA. We used muffin-tin spheres around each element in the double perovskites under study. In this case, we used the LAPW basis set to expand the wave functions so that the waves within the spheres would be atomistic, while those outside would be plane waves. For better convergence, we used l_{max} = 10 and R_{MT} x K_{max} = 8, respectively. We performed this electronic structure treatment using the Wien2k model. We analyzed transport properties up to 4000 k-points using BoltzTraP [39].

3. Results and Discussion

3.1 Structural properties

This paper explores the structure of the halide double perovskite material A_2BX_6 (A = Cs; B = Ge; X = Cl, Br), which adopts a face-centered cubic structure with the space group of Fm3m (No. 225). Figures 1a and 1b depict the atomic structure of A_2BX_6 (A = Cs; B = Ge; X = Cl, Br), showing the system's exact geometry. These figures depict the structures of vacancy-ordered double perovskites Cs_2GeCl_6 and Cs_2GeBr_6 with different chromium doping levels (Cr: 0%, Ge: 75%, Cr: 25%). Both structures have a face-centered cubic shape. Throughout the calculation, the Fm-3m (225) space group is employed. Atomic locations of Cs (0.25, 0.25, 0.25), Ge (0.00, 0.00, 0.00), and Cl, Br (0.20, 0.00, 0.00) are utilized [40], and chromium concentration vary with controlling Ge concentration, as seen in Figure 1 (a & b). With increasing chromium doping concentration, the lattice parameters of Cs_2GeCl_6 and Cs_2GeBr_6 increase. The computed lattice parameters are: Cs_2GeCl_6: 10.32 Å, $Cs_2Ge_{0.75}Cr_{0.25}Cl_6$:10.55 Å, Cs_2GeBr_6: 10.65 Å, and $Cs_2Ge_{0.75}Cr_{0.25}Br_6$: 10.85 Å. Furthermore, Figure 1 (a & b) depict B-lacking ABX_3 perovskites with BX6 octahedra. The A-site atoms contribute to the filling of empty spaces between octahedra. Each [BX_6] octahedron in the A_2BX_6 structure is isolated, resulting in a 12-fold coordinated framework of different X anions. A-atoms (cations) are bounded by 12 Cl, Br halogen ions, whereas the B-atoms are surrounded by 6 Cl, Br halogen ions. The BX_6 octahedra are essential to forming the cubic structure. Before and after doping, all structures are cubic. The computed necessary optimal information is presented in Table 1, using the GGA-PBE technique. No theoretical or experimental studies are available for comparison. Furthermore, to check the stability of the current materials, the stability and octahedral factor play a vital role. The following relations are used to determine the tolerance factor and octahedral factor [41]:

$$\text{Tolerance factor} = t = \frac{r_A + r_X}{\sqrt{2}(r_B + r_X)} \quad (1)$$

$$\text{Octahedral factor} = \mu = \frac{r_B}{r_X} \quad (2)$$

Here r sub cap A, r sub cap B, and r sub cap X are the corresponding ionic radii of the A, B, and X atoms in the BX_3 perovskite structure. Perovskite crystals exhibit excellent cubic shapes when t = 1. The octahedral factor is another technique used to describe structural stability. Tolerance and octahedral factors are empirical systems that ignore chemical interactions between constituents. As a result, the largest stability domain of ABX_3 varies with the chemical composition of the components. The perovskite structure is expected to be achieved in the halide perovskites if the tolerance factor t falls between 0.813 and 1.107 and

0.442 and 0.895. The estimation of tolerance and octahedral factors assumes that all ions, including the organic ones, are perfect hard spheres and that ionic radii do not depend on temperature. However, estimating perovskite stability using tolerance and octahedral factors can be relatively easy and instructive. In the current work, perovskite crystal stability is estimated using both tolerance and octahedral criteria. It is related to ABX_3 type perovskite systems where ions A, B, and X have coordination numbers 12, 6, and 6, respectively. Ionic radii for B and X ions are taken from Shannon. The ionic radii of A-site cations are taken as constraints because Shannon's classification system provides no complete data for 12-coordinate ions. The tolerance and octahedral factors were calculated using these values r_A= 1.88 Å, r_B= 0.73 Å, r_{Cl}= 1.81 Å, and r_{Br}=1.96 Å, r_{Cr}=0.80 Å (Tanaka, Oku, & Ueoka, 2018). The calculated values are: Cs_2GeCl_6: t= 1.02, μ= 0.40 and Cs_2GeBr_6: t= 1.01, μ= 0.37. Therefore, the following structures are stable because these values meet the required stability criteria.

Table 1: Calculated parameters for $Cs_2Ge_{1-x}Cr_xX_6$ (x= 0, 0.25).

Compound	a_o(Å)	B_o(GPa)	ΔH_f (eV)	E_g (eV)	M_{tot}	M_{Cr}	M_{Cs}	M_{Ge}	$M_{Cl/Br}$
Cs_2GeCl_6	10.32	64.31	-2.45	4.5	-	-	-	-	-
$Cs_2Ge_{0.75}Cr_{0.25}Cl_6$	10.55	52.16	-2.24	4.1	3.000	0.632	-0.009	0.2584	1.500
Cs_2GeBr_6	10.65	48.42	-2.30	3.0	-	-	-	-	-
$Cs_2Ge_{0.75}Cr_{0.25}Br_6$	10.85	36.46	-2.15	2.5	3.000	0.650	-0.007	0.2650	1.650

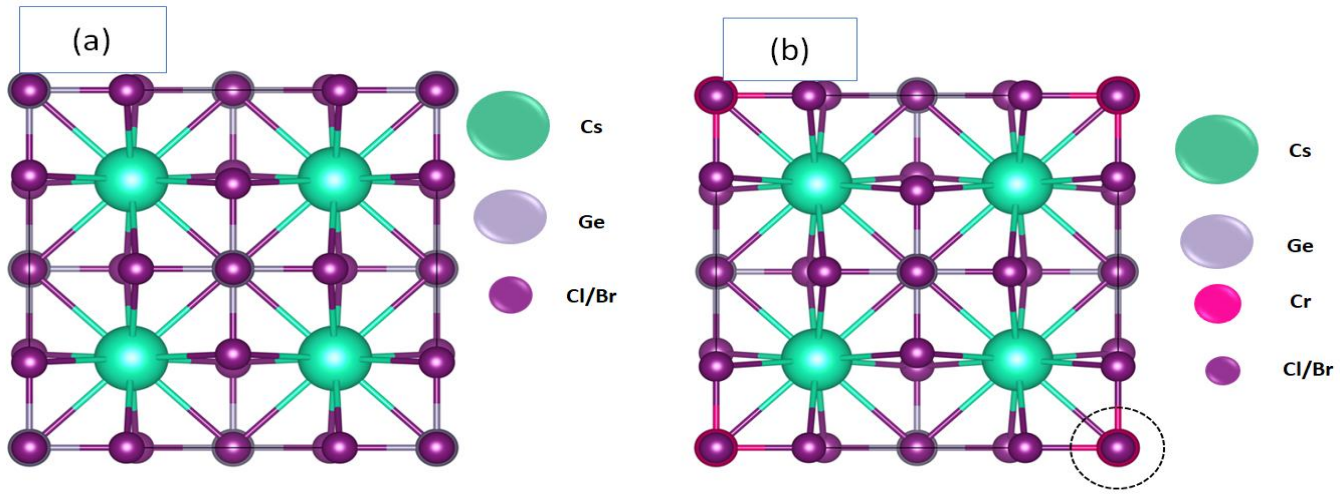

Fig. 1: Optimized cubic crystal structures of A_2BX_6 (A=Cs; B=Ge; X=Cl, Br)

We used formation energies to study the thermodynamic stability of A_2BX_6 perovskites (A = Cs; B = Ge; X = Cl, Br) along all possible synthesis routes. Formation energy is the energy difference between the total energy of the compound and the sum of the energies of its individual elemental constituents [42]. Therefore, it is calculated as follows:

$$\Delta H_f = E_t^{A_2BX_6} - 2E_t^{A_{cubic}} - E_t^{B_{cubic}} - 6E_t^{X_{ortho}} \quad (3)$$

Where $E_t^{A_2BX_6}$, E_t^A, E_t^B, and E_t^X denote ground-state total energies of A_2BX_6, compound, and elemental components A, B, and X in their most thermodynamically stable standard structures, respectively. We carried out a comprehensive geometry optimization for each system under consideration, i.e., locating the volume at which the material's energy is lowest. When describing the stability of a compound, the sign and size of its formation energy are most often cited in the literature, as we have seen. When the formation energy is negative, the material is stable; a positive value indicates that the compound is unstable and cannot be synthesized at room temperature and pressure. More negative formation energy means a more stable Proofreadingmolecule, and vice versa. Table 1 summarizes the formation energy data for all chosen contenders. Our findings suggest that these materials have a negative formation energy, indicating that they are more stable. Table 1 compares the $Cs_2Ge_{1-x}Cr_xX_6$ (x = 0, 0.25) perovskites; Cs_2GeCl_6 is the most stable. After Cr doping, the stability of both Cs_2GeCl_6 and Cs_2GeBr_6 perovskites declines, although the former is still more stable than the latter.

3.2 Electronic properties

To explain the electronic behavior, we studied the spin-polarized band structure, total density of states (TDOS), and partial density of states (PDOS) for $Cs_2Ge_{1-x}Cr_xX_6$ compounds at x = 0 and x = 0.25. The results of spin-

dependent band structure and TDOS for both the spin-up and spin-down configurations are illustrated in Figures 2-4, where spin-dependent PDOS is also segregated in terms of atomic contribution as well as orbital contribution. The calculated band gap energies are 4.5 eV for Cs_2GeCl_6, 4.1 eV for $Cs_2Ge_{0.75}Cr_{0.25}Cl_6$, 3.0 eV for Cs_2GeBr_6, and 2.5 eV for $Cs_2Ge_{0.75}Cr_{0.25}Br_6$.

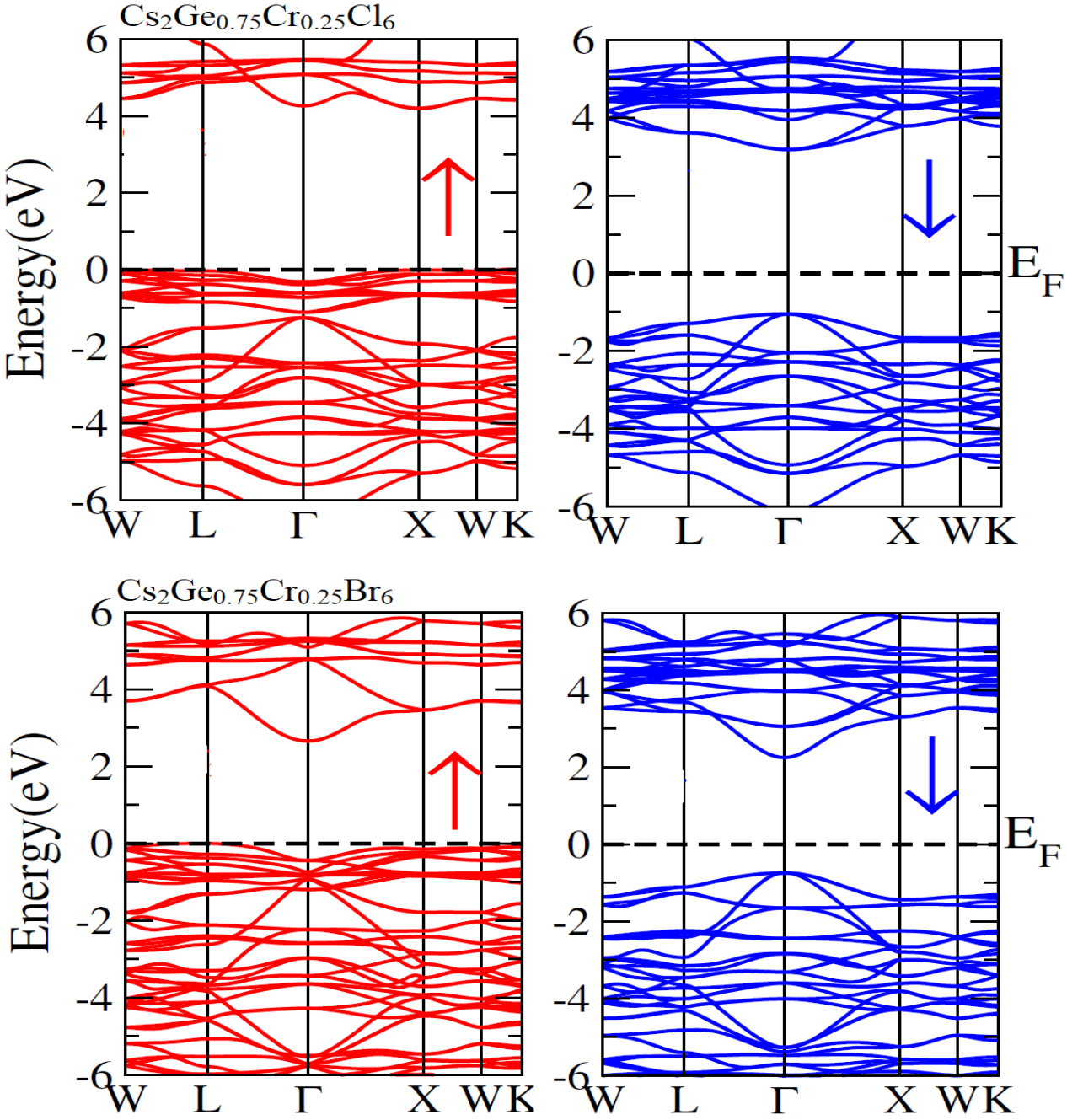

Fig. 2: Band structures of $Cs_2Ge_{0.75}Cr_{0.25}Cl_6$ and $Cs_2Ge_{0.75}Cr_{0.25}Br_6$ with up-spin and down-spin channels

The electron transition can be understood using electronic features. Fermi level EF is set to 0.0 eV. The total and partial DOSs for spin-up and spin-down channels are also investigated using GGA with the PBE exchange-correlation functional. In the current scenario, the $Cs_2Ge_{0.75}Cr_{0.25}Cl_6$ and $Cs_2Ge_{0.75}Cr_{0.25}Br_6$ show an indirect band gap nature with spin-up, while with spin-down they exhibit a direct nature, as represented in Figure 2. The energy band gap values for the eight A_2BX_6 perovskite materials have been calculated and are provided in Table 1 below. This is as part of a systematic study to establish whether they satisfy the required condition in terms of their electronic structure. Table 1 lists the band-gap values for all materials calculated with different exchange-correlation functionals.

Figure 2 provides electronic band structure diagrams for A_2BX_6 perovskites using the GGA-PBE approximation, plotted along high-symmetry points in the Brillouin Zone, while keeping the A-site cation constant in all cases. The band structures show that all materials considered here behave as semiconductors. Notably, in the cases of undoped and 25% Cr doped Cs_2GeCl_6/Br_6 materials, indirect band gaps are expected, as shown in Figure 2 below. In such cases, the valence band maximum and conduction band minimum are located at a high-symmetry point (0.0, 0.0, 0.0).

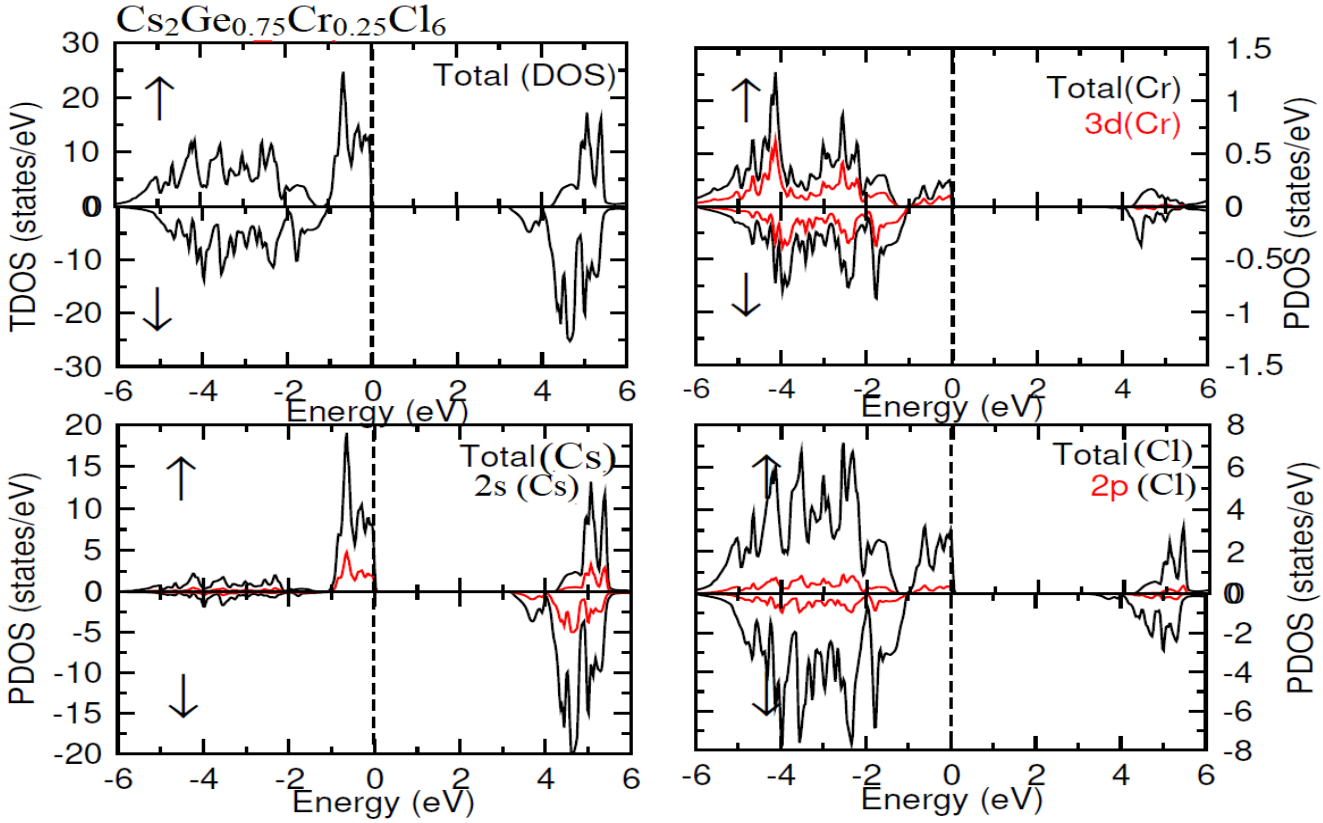

Fig. 3: Total and partial DOSs of $Cs_2Ge_{0.75}Cr_{0.25}Cl_6$with up-spin and down-spin channels

Figure 2 shows that anti-bonding orbitals of Ge-5s and X-5p are responsible for most of the valence band, whereas those of Ge-5p are responsible for all of the conduction band. Cs-2s, Cr-3d, Cl-, and Br-2p orbitals hybridize below and above the Fermi level, respectively, in the TDOS and PDOS for $Cs_2Ge_{1-x}Cr_xX_6$ (x = 0, 0.25), and the high peaks between -1.5 and 6 eV indicate hybridization between the Cl-, Br-2p, and Cs-2s orbitals. Significant hybridization of the Cs-2s, Cr-3d, and Cl-, Br-4p orbitals causes peaks below the Fermi threshold. Cs_2GeCl_6 and Cs_2GeBr_6 are both pure semiconductors, but Cs_2GeCl_6 with 25% Cr-doping at the Ge site is also a semiconductor (as shown by the DOS graphs). The PDOS of halide perovskites elucidates the role of each orbital in the band structures and reveals evidence of hybridization inside the double halide lead-free perovskites. Figures 3 and 4 show the PDOS (with 25% Cr doping) for $Cs_2Ge_{0.75}Cr_{0.25}Cl_6$ and $Cs_2Ge_{0.75}Cr_{0.25}Br_6$. The PDOS analysis suggests that the valence band maximum is mainly composed of contributions from the p states of Cl/Br, but also shows significant mixing with Cr 3d states, indicating strong covalent bonding between chromium and the halide elements. In contrast, the conduction-band minimum is mainly dominated by Cr 3d states, while the involvement of Cs states near the band edge is insignificant. The energy range of -4 eV to 0.0 eV is classified as the upper valence band region, while the energy range of 0.0 eV to 4 eV belongs to the lower conduction band region. As seen in Figures 3 and 4, the sum of Cl spin-up and spin-down channels is the major contributor to the formation of the valence band edge compared to the contributions of other orbital channels. Similarly, the sum of Cl spin-up and spin-down channels largely determines the conduction band edge, while other channels contribute little. Adding Cr further increases their relative contributions. Incorporating Cr creates localized 3d electronic states that strongly hybridize with neighboring anion p-orbitals, changing the electronic band dispersion near the Fermi level. Hybridization decreases the band gap and increases spin polarization, which is desired for spintronics. It has also been discussed that the extent of band-gap modification depends on the exchange interaction and crystal-field splitting of Cr 3d states [43].

3.3 *Magnetic properties*

In the context of magnetic properties, various magnetic attributes (M_{tot}, M_{Cs}, $M_{Cl/Br}$, M_{Ge}, M_{Cr}) are calculated and recorded in Table 1. Figures 2, 3, and 4 show the band structures, TDOS, and PDOS for $Cs_2Ge_{0.75}Cr_{0.25}Cl_6$ and $Cs_2Ge_{0.75}Cr_{0.25}Br_6$. We then evaluate the magnetic moment using the GGA + mBJ potential approach and discuss the atomic contributions. Ferromagnetic semiconductor nature materials are characterized by a magnetism that has an integral value of $3\mu_B$, as discovered by the (GGA + mBJ) schemes. The highest number of half-filled p-states in $M_{Cl/Br}$ atoms is clearly seen in the magnetism inside the structure [44]. Other elements' (not stated above) small contribution to the total magnetic moment is reflected in their low-lying energy levels, which are distant from the Fermi level. Cl and Br atoms are most visible close to the Fermi level, but fade away at 25% Cr doping, which is reflected in the PDOS calculated using the GGA + mBJ functional scheme. Table 1 shows the results of our calculations for the total and individual magnetic moments of the atoms.

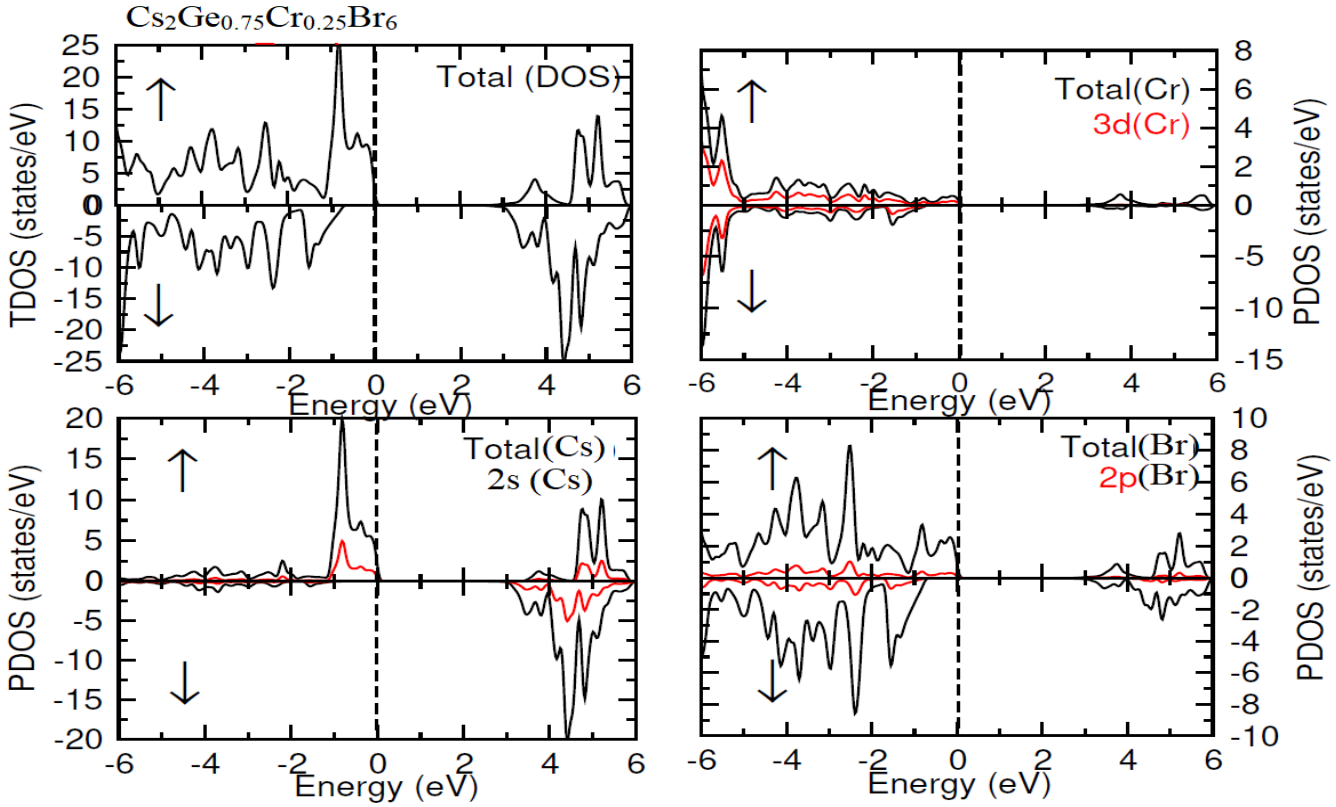

Fig.4: TDOS and PDOS of $Cs_2Ge_{0.75}Cr_{0.25}Br_6$with up-spin and down-spin channels

3.4 *Thermoelectric properties*

This band structure determines how a material will behave under thermoelectric conditions, making band gap engineering very effective for this purpose. Thermoelectric (TE) materials can convert wasted energy into useful forms. Currently, because of their ability to control energy convergence, these materials are being studied much faster than other technological materials [45]. The thermoelectric transport properties were calculated using the BoltzTraP software tool, which uses the semiclassical Boltzmann transport equations in the constant relaxation time approximation (CRTA). Both of these calculations are performed using the band structure data obtained from the first-principles calculations, where an energy-independent relaxation time (τ) is used, along with the rigid band approximation to account for doping effects. In such a case, the Seebeck coefficient (S) does not depend on τ, whereas the electrical conductivity (σ) and electronic thermal conductivity (κ_e) are given by σ/τ and κ_e/τ, respectively. As per the usual protocol followed in the BoltzTraP calculations, no scattering process is taken into account. Thermopower is the amount of electromotive force produced by a material under certain thermal gradients. Thermopower is used to determine how effective a material will be under thermoelectric conditions, and since it depends on the band structure, it determines electron and phonon transport [46]. ZT, a quantity that is dimensionless, represents the figure of merit of the thermoelectric process and is given by $ZT=S^2T\sigma/\kappa$ is a quantity independent of both time and space and varies proportionally to $S\sigma T$. Specifically, $\kappa = \kappa_l + \kappa_{el}$ describes the relationship between thermal conductivity κ and specific heat capacity of material. Successful solutions for fine-tuning these transport parameters need knowledge of electron-phonon transport interactions in a typical TE material. In terms of Boltzmann transport theory, a number of transport coefficients, namely, electrical conductivity, normalized Seebeck coefficient, electronic and lattice

thermal conductivities, as well as power factor, have been calculated to study the electronic transport characteristics of the layered $Cs_2Ge_{1-x}Cr_xX_6$ (x = 0, 0.25) perovskites within the assumptions of the constant relaxation time and rigid band approximations [47]. These transport coefficients include electrical conductivity (σ/τ), Seebeck coefficient (S), and total thermal conductivity (κ_{total}), among others. The results are shown in Figures 5(a) and 6(a, b).

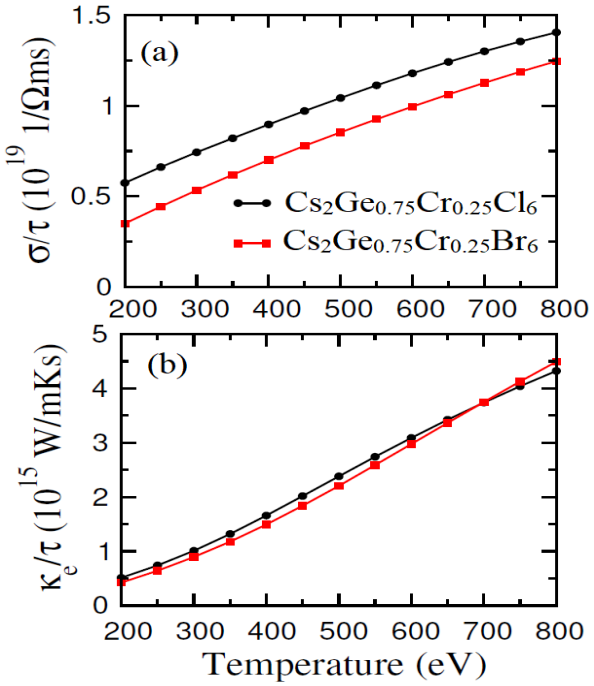

Fig. 5: (a) Electrical conductivity, and (b) thermal conductivity of $Cs_2Ge_{0.75}Cr_{0.25}Cl_6$ and $Cs_2Ge_{0.75}Cr_{0.25}Br_6$

Compounds are either p- or n-type depending on the number of electrons or holes present in the valence and conduction bands, respectively. When calculating the thermoelectric characteristics of $Cs_2Ge_{1-x}Cr_xX_6$ (x = 0, 0.25) double perovskites, the Boltz trap algorithm is employed (see methodology part). The electrical conductivity for the $Cs_2Ge_{0.75}Cr_{0.25}Cl_6$ and $Cs_2Ge_{0.75}Cr_{0.25}Br_6$ are shown by Figure 5(a). The calculated values from the graph 5(a) for $Cs_2Ge_{0.75}Cr_{0.25}Cl_6$ is $\sigma/\tau = 0.60 \times 10^{19}(\Omega ms)^{-1}$ and for $Cs_2Ge_{0.75}Cr_{0.25}Br_6$ is $\sigma/\tau = 0.30 \times 10^{19}(\Omega ms)^{-1}$ at 200 K temperature. To enhance the electrical conductivity, the temperature must rise, since more carriers are made available in the conduction band at higher temperatures. At 800 K temperature, for $Cs_2Ge_{0.75}Cr_{0.25}Cl_6$ is $\sigma/\tau = 1.40 \times 10^{19}(\Omega ms)^{-1}$ and for $Cs_2Ge_{0.75}Cr_{0.25}Br_6$ is $\sigma/\tau = 1.25 \times 10^{19}(\Omega ms)^{-1}$. Furthermore, the two modes of heat conduction are the electron and the phonon, and the thermal conductivity relationship is given by $\kappa = \kappa_{electron} + \kappa_{phonon}$, where κ_{phonon} phonon and $\kappa_{electron}$ are the phononic and electronic thermal conductivity coefficients, respectively. To avoid issues with the BoltzTraP algorithm, we considered only the electronic contribution to thermal conductivity and ignored lattice vibrations [48]. Figure 5(b) shows the current thermal conductivity values. The calculated values are: for $Cs_2Ge_{0.75}Cr_{0.25}Cl_6$ is $\kappa_{electron}/\tau = 0.50 \times 10^{15} W/Kms$ and for $Cs_2Ge_{0.75}Cr_{0.25}Br_6$ is $\kappa_{electron}/\tau = 0.40 \times 10^{15} W/Kms$ at 200 K temperature. The exponential growth is found in thermal conductivity which can be observed from Figure 5(b). At 800 K temperature, its values are: $\kappa_{electron}/\tau = 4.40 \times 10^{15} W/Kms$ and for $Cs_2Ge_{0.75}Cr_{0.25}Br_6$ is $\kappa_{electron}/\tau = 4.50 \times 10^{15} W/Kms$. The value of the band gap explains the slight increase in the thermal conductivity value. The value of the electronic thermal conductivity to the relaxation time, κ_e/τ, is still about 10^{-5}. Overall, the calculated values suggest that the studied materials can be used for thermoelectric devices.

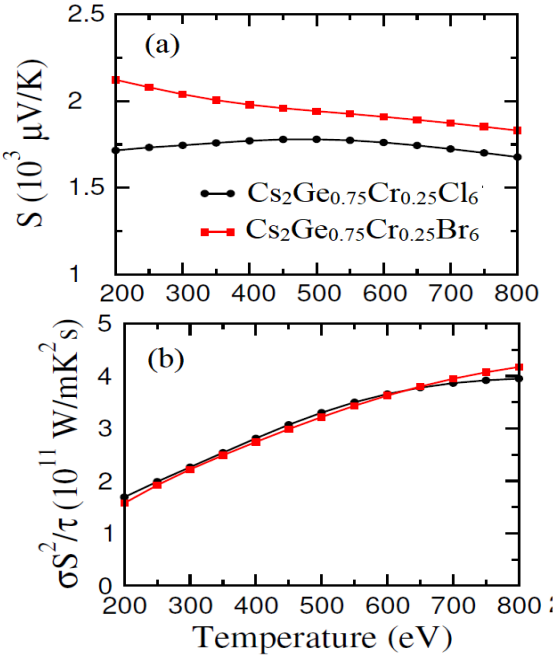

Fig. 6: (a) Seebeck-coefficient (b) Figure of merit of $Cs_2Ge_{0.75}Cr_{0.25}Cl_6$ and $Cs_2Ge_{0.75}Cr_{0.25}Br_6$

In a thermoelectric system, the temperature difference between two metallic junctions creates a voltage difference, and the Seebeck coefficient, S, determines its effect on device efficiency. In Fig. 6a, the Seebeck coefficient decreases monotonically with temperature in the range 200-800 K, suggesting that carrier excitation increases as thermopower decreases. Given the positive sign, this material is a p-type semiconductor in which holes are responsible for charge transport. It can be noted that the values of the thermoelectric parameters found correspond very well to the electronic structure. The large value of the Seebeck coefficient comes from the semiconducting nature of the materials, as well as the presence of the sharp density of states peaks at the band edges. Electrical conductivity depends on the dispersion of the bands near the Fermi level; the larger the dispersion, the higher the conductivity.

It should be noted that the temperature dependence of the electronic thermal conductivity corresponds to the dependence of electrical conductivity, since both are associated with charge-carrier motion according to the

Wiedemann-Franz law. Computed Seebeck coefficients of $Cs_2Ge_{0.75}Cr_{0.25}Cl_6$ and $Cs_2Ge_{0.75}Cr_{0.25}Br_6$ at 200 K have the values of 1.73 and 2.13 μV/K, respectively. At 800 K, these same materials yield Seebeck coefficients of 1.70 μV/K and 1.80 μV/K for $Cs_2Ge_{0.75}Cr_{0.25}Cl_6$ and $Cs_2Ge_{0.75}Cr_{0.25}Br_6$, respectively. The material $Cs_2Ge_{0.75}Cr_{0.25}Br_6$ has relatively large Seebeck coefficients compared with those of $Cs_2Ge_{0.75}Cr_{0.25}Cl_6$ due to Coulomb interaction and bond dissociation effects. In thermoelectricity, two main parameters determine a material's efficiency in energy generation: electrical conductivity and the Seebeck coefficient, commonly represented by the power factor ($PF/\tau = S^2\sigma/\tau$). The power factor (PF) of thermoelectricity was also examined with respect to the temperature regime, as shown in Fig. 6(b). There are two states in the first phase from 200-650 K temperature; it increases, and from 650-800 K temperature, it increases for $Cs_2Ge_{0.75}Cr_{0.25}Br_6$ and decreases for $Cs_2Ge_{0.75}Cr_{0.25}Cl_6$, as represented in Figure 6(b). The calculated values of $Cs_2Ge_{0.75}Cr_{0.25}Cl_6$ and $Cs_2Ge_{0.75}Cr_{0.25}Br_6$ at 200 K are PF=$1.90\times 10^{11} W/K^2ms$ and $1.85 \times 10^{11} W/K^2ms$, respectively. At 800 K, ZT= $3.98\times 10^{11} W/K^2ms$ $Cs_2Ge_{0.75}Cr_{0.25}Cl_6$ and $4.09\times 10^{11} W/K^2ms$ $Cs_2Ge_{0.75}Cr_{0.25}Br_6$. Additionally, we calculate the room temperature values of ZT by employing the formula as $ZT=\sigma S^2T/\kappa$. Room temperature ZT values are 0.79 and 0.78 for $Cs_2Ge_{0.75}Cr_{0.25}Cl_6$ and $Cs_2Ge_{0.75}Cr_{0.25}Br_6$, respectively indicating both doped compositions are potentially used in thermoelectric devices.

4. Conclusions

In the current research, density functional theory (DFT) using FP-LAPW+lo method is applied to investigate structural, magnetic, thermoelectric, and electronic properties of the studied materials. In this study, DFT calculations were performed on the physical properties of A_2BX_6 halides (A = Cs, B = Ge, X = Cl, Br) with or without Cr substitution. Our calculated results indicate as the chromium doping ratio rises, the equilibrium lattice parameters of Cs_2GeCl_6 and Cs_2GeBr_6 also increase. The computed lattice parameters are Cs_2GeCl_6: 10.32 Å, $Cs_2Ge_{0.75}Cr_{0.25}Cl_6$: 10.55 Å, and Cs_2GeBr_6: 10.65Å, $Cs_2Ge_{0.75}Cr_{0.25}Br_6$: 10.85Å. The formation energy and tolerance factor criteria promote structural and thermodynamic stability. The computed band gap for Cs_2GeCl_6 is 4.5 eV, $Cs_2Ge_{0.75}Cr_{0.25}Cl_6$ is 4.1 eV, Cs_2GeBr_6 is 3.0 eV, and $Cs_2Ge_{0.75}Cr_{0.25}Br_6$ is 2.5 eV. $Cs_2Ge_{0.75}Cr_{0.25}Cl_6$ and $Cs_2Ge_{0.75}Cr_{0.25}Br_6$ exhibit an indirect band gap. With 25% Cr doping, the total magnetic moments of $Cs_2Ge_{0.75}Cr_{0.25}Cl_6$ and $Cs_2Ge_{0.75}Cr_{0.25}Br_6$ are identical. Hence, the studied compounds have good prospects for use in optoelectronics, which includes solar cells. The figure of merit is calculated to be 0.79 for $Cs_2Ge_{0.75}Cr_{0.25}Cl_6$ and 0.78 for $Cs_2Ge_{0.75}Cr_{0.25}Br_6$, pointing out that these compounds can be used as thermoelectric materials. It should be emphasized that the Seebeck coefficient is negative.

References

[1] Q. A. Akkerman and L. Manna, "What defines a halide perovskite?" *ACS Energy Lett.*, pp. 604–610, 2020, doi: 10.1021/acsenergylett.0c00039.

[2] Q. Tai, K. C. Tang, and F. Yan, "Recent progress of inorganic perovskite solar cells," *Energy Environ. Sci.*, vol. 12, pp. 2375–2405, 2019, doi: 10.1039/C9EE01479A.

[3] R. Wang, M. Mujahid, Y. Duan, Z. K. Wang, J. Xue, and Y. Yang, "A review of perovskites solar cell stability," *Adv. Funct. Mater.*, vol. 29, pp. 1–25, 2019, doi: 10.1002/adfm.201808843.

[4] J. Zhang, Z. Zhao, Z. Xia, and L. Dai, "A metal-free bifunctional electrocatalyst for oxygen reduction and oxygen evolution reactions," *Nat. Nanotechnol.*, vol. 10, pp. 444–452, 2015, doi: 10.1038/nnano.2015.48.

[5] T. R. Cook, D. K. Dogutan, S. Y. Reece, Y. Surendranath, T. S. Teets, and D. G. Nocera, "Solar energy supply and storage for the legacy and nonlegacy worlds," *Chem. Rev.*, vol. 110, pp. 6474–6502, 2010.

[6] A. E. Fedorovskiy, N. A. Drigo, and M. K. Nazeeruddin, "The role of Goldschmidt's tolerance factor in the formation of A_2BX_6 double halide perovskites and its optimal range," *Small Methods*, vol. 4, pp. 1–6, 2020, doi: 10.1002/smtd.201900426.

[7] G. Catalan and J. F. Scott, "Physics and applications of bismuth ferrite," *Adv. Mater.*, vol. 21, pp. 2463–2485, 2009, doi: 10.1002/adma.200802849.

[8] M. Ju, M. Chen, Y. Zhou, H. F. Garces, J. Dai, L. Ma, N. P. Padture, and X. C. Z. Minggang, "Earth-abundant nontoxic titanium(IV)-based vacancy-ordered double perovskite halides with tunable 1.0 to 1.8 eV bandgaps for photovoltaic applications," *ACS Energy Lett.*, vol. 3, pp. 297–304, 2018, doi: 10.1021/acsenergylett.7b01167.

[9] P. K. Kung, M. H. Li, P. Y. Lin, J. Y. Jhang, M. Pantaler, D. C. Lupascu, G. Grancini, and P. Chen, "Lead-free double perovskites for perovskite solar cells," *Sol. RRL*, vol. 4, 2020, doi: 10.1002/solr.201900306.

[10] S. Thawarkar, S. R. Rondiya, N. Y. Dzade, N. Khupse, S. Jadkar, "Experimental and theoretical investigation of the structural and opto-electronic properties of Fe-doped lead-free $Cs_2AgBiCl_6$ double perovskite," *Chem. Eur. J.*, vol. 27, pp. 7408–7417, 2021, doi: 10.1002/chem.202004902.

[11] A. Kojima, K. Teshima, Y. Shirai, and T. Miyasaka, "Organometal halide perovskites as visible-light sensitizers for photovoltaic cells," *J. Am. Chem. Soc.*, vol. 131, pp. 6050–6051, 2009, doi: 10.1021/ja809598r.

[12] W. Xu, Q. Hu, S. Bai, C. Bao, Y. Miao, Z. Yuan, T. Borzda, A. J. Barker, E. Tyukalova, Z. Hu, M. Kawecki, H. Wang, Z. Yan, X. Liu, X. Shi, K. Uvdal, M. Fahlman, W. Zhang, M. Duchamp, J. M. Liu, A. Petrozza, J. Wang, L. M. Liu, W. Huang, and F. Gao, "Rational molecular passivation for high-performance perovskite light-emitting diodes," *Nat. Photonics*, vol. 13, pp. 418–424, 2019, doi: 10.1038/s41566-019-0390-x.

[13] L. Chu, W. Ahmad, W. Liu, J. Yang, R. Zhang, Y. Sun, J. Yang, and X. Li, "Lead-free halide double perovskite materials: A new superstar toward green and stable optoelectronic applications," *Nano-Micro Lett.*, vol. 11, 2019, doi: 10.1007/s40820-019-0244-6.

[14] M. I. Khan, G. Hassan, M. S. Hasan, S. A. Abubshait, H. A. Abubshait, W. Al-Masry, Q. Mahmood, A. Mahmood, and S. M. Ramay, "Investigations on the efficiency variation of zinc and gallium co-doped TiO_2 based dye sensitized solar cells," *Ceram. Int.*, vol. 46, pp. 24844–24849, 2020, doi: 10.1016/j.ceramint.2020.06.268.

[15] Q. Mahmood, T. H. Flemban, H. Althib, T. Alshahrani, M. G. B. Ashiq, B. Ul Haq, Y. Tahir, A. Surrati, N. A. Kattan, and A. Laref, "The study of optical and thermoelectric properties of lead-free variant iodides $(K/Rb)_2TiI_6$," *J. Mater. Res. Technol.*, vol. 9, pp. 13043–13053, 2020, doi: 10.1016/j.jmrt.2020.09.046.

[16] R. Ali, G. J. Hou, Z. G. Zhu, Q. B. Yan, Q. R. Zheng, and G. Su, "Predicted lead-free perovskites for solar cells," *Chem. Mater.*, vol. 30, pp. 718–728, 2018, doi: 10.1021/acs.chemmater.7b04036.

[17] T. I. Al-Muhimeed, A. Shafique, A. A. AlObaid, M. Morsi, G. Nazir, M. Mana Al-Anazy, and Q. Mahmood, "New lead-free double perovskites X_2GeI_6 (X = K, Rb, Cs) for solar cells, and renewable

energy as an alternate of hybrid perovskites," *Int. J. Energy Res.*, vol. 45, pp. 19645–19652, 2021, doi: 10.1002/er.7022.

[18] G. Flora, D. Gupta, and A. Tiwari, "Toxicity of lead: A review with recent updates," *Interdiscip. Toxicol.*, vol. 5, pp. 47–58, 2012, doi: 10.2478/v10102-012-0009-2.

[19] S. Berri, "Thermoelectric properties of A_2BCl_6: A first-principles study," *J. Phys. Chem. Solids*, vol. 170, Art. no. 110940, 2022, doi: 10.1016/j.jpcs.2022.110940.

[20] F. Hao, C. C. Stoumpos, R. P. H. Chang, and M. G. Kanatzidis, "Anomalous band gap behavior in mixed Sn and Pb perovskites enables broadening of absorption spectrum in solar cells," *J. Am. Chem. Soc.*, vol. 136, pp. 8094–8099, 2014, doi: 10.1021/ja5033259.

[21] T. Krishnamoorthy, H. Ding, C. Yan, W. L. Leong, T. Baikie, Z. Zhang, M. Sherburne, S. Li, M. Asta, N. Mathews, and S. G. Mhaisalkar, "Lead-free germanium iodide perovskite materials for photovoltaic applications," *J. Mater. Chem. A*, vol. 3, pp. 23829–23832, 2015, doi: 10.1039/C5TA05741H.

[22] J. C. Hebig, I. Kühn, J. Flohre, and T. Kirchartz, "Optoelectronic properties of $(CH_3NH_3)_3Sb_2I_9$ thin films for photovoltaic applications," *ACS Energy Lett.*, vol. 1, pp. 309–314, 2016, doi: 10.1021/acsenergylett.6b00170.

[23] T. Singh, A. Kulkarni, M. Ikegami, and T. Miyasaka, "Effect of electron transporting layer on bismuth-based lead-free perovskite $(CH_3NH_3)_3Bi_2I_9$ for photovoltaic applications," *ACS Appl. Mater. Interfaces*, vol. 8, pp. 14542–14547, 2016, doi: 10.1021/acsami.6b02843.

[24] M. T. Klug, A. Osherov, A. A. Haghighirad, S. D. Stranks, P. R. Brown, S. Bai, J. T. W. Wang, X. Dang, V. Bulović, H. J. Snaith, and A. M. Belcher, "Tailoring metal halide perovskites through metal substitution: Influence on photovoltaic and material properties," *Energy Environ. Sci.*, vol. 10, pp. 236–246, 2017, doi: 10.1039/C6EE03201J.

[25] Y. Hu, T. Qiu, F. Bai, X. Miao, and S. Zhang, "Enhancing moisture-tolerance and photovoltaic performances of $FAPbI_3$ by bismuth incorporation," *J. Mater. Chem. A*, vol. 5, pp. 25258–25265, 2017, doi: 10.1039/C7TA08824H.

[26] M. A. Green, A. Ho-Baillie, and H. J. Snaith, "The emergence of perovskite solar cells," *Nat. Photonics*, vol. 8, pp. 506–514, 2014, doi: 10.1038/nphoton.2014.134.

[27] M. Saliba, S. Orlandi, T. Matsui, S. Aghazada, M. Cavazzini, J. P. Correa-Baena, P. Gao, R. Scopelliti, E. Mosconi, K. H. Dahmen, F. De Angelis, A. Abate, A. Hagfeldt, G. Pozzi, M. Grätzel, and M. K. Nazeeruddin, "A molecularly engineered hole-transporting material for efficient perovskite solar cells," *Nat. Energy*, vol. 1, pp. 1–7, 2016, doi: 10.1038/nenergy.2015.17.

[28] V. Malgras, A. Nattestad, J. H. Kim, S. X. Dou, and Y. Yamauchi, "Understanding chemically processed solar cells based on quantum dots," *Sci. Technol. Adv. Mater.*, vol. 18, pp. 334–350, 2017, doi: 10.1080/14686996.2017.1317219.

[29] A. E. Maughan, A. M. Ganose, M. M. Bordelon, E. M. Miller, D. O. Scanlon, and J. R. Neilson, "Defect tolerance to intolerance in the vacancy-ordered double perovskite semiconductors Cs_2SnI_6 and Cs_2TeI_6," *J. Am. Chem. Soc.*, vol. 138, pp. 8453–8464, 2016, doi: 10.1021/jacs.6b03207.

[30] M. D. I. Bhuyan, R. Hossain, F. Ara, and M. A. Basith, "A first-principles study on the phase stability and physical properties of a B-site ordered Nd_2CrFeO_6 double perovskite," *Phys. Chem. Chem. Phys.*, vol. 24, pp. 1569–1579, 2022.

[31] Kumawat, M. Rani, D. K. Meena, Anuradha, K. Kumar, and G. Arora, "Electronic, optical and magnetic properties of Gd_2FeCrO_6 double perovskite using DFT," *Mater. Today Proc.*, 2023.

[32] Q. Mahmood, T. Ghrib, A. Rached, A. Laref, and M. A. Kamran, "Probing of mechanical, optical and thermoelectric characteristics of double perovskites Cs_2GeCl/Br_6 by DFT method," *Mater. Sci. Semicond. Process.*, vol. 112, Art. no. 105009, 2020, doi: 10.1016/j.mssp.2020.105009.

[33] M. Faizan, S. H. Khan, H. Khachai, T. Seddik, S. Bin Omran, R. Khenata, J. Xie, M. Mana Al-Anazy, "Electronic, optical, and thermoelectric properties of perovskite variants A_2BX_6: Insight and design via first-principles calculations," *Int. J. Energy Res.*, vol. 45, pp. 4495–4507, 2021, doi: 10.1002/er.6118.

[34] M. G. Brik and I. V. Kityk, "Modeling of lattice constant and their relations with ionic radii and electronegativity of constituting ions of A_2XY_6 cubic crystals (A = K, Cs, Rb, Tl; X = tetravalent cation, Y = F, Cl, Br, I)," *J. Phys. Chem. Solids*, vol. 72, pp. 1256–1260, 2011, doi: 10.1016/j.jpcs.2011.07.016.

[35] M. Asghar, M. Zanib, M. A. Khan, S. Niaz, N. A. Noor, and A. Dahshan, "Tuning of the bandgap of Rb_2ScAgX_6 (X = Cl, Br, I) double perovskites through halide ion replacement for solar cell applications," *Mater. Sci. Semicond. Process.*, vol. 148, Art. no. 106819, 2022, doi: 10.1016/j.mssp.2022.106819.

[36] P. Blaha, K. Schwarz, G. K. H. Madsen, D. Kvasnicka and J. Luitz, WIEN2k: An Augmented Plane Wave + Local Orbitals Program for Calculating Crystal Properties, Vienna University of Technology, Vienna, Austria, 2001.

[37] J. P. Perdew, K. Burke and M. Ernzerhof, Generalized Gradient Approximation Made Simple, Phys. Rev. Lett., 1996, 77, 3865–3868.

[38] F. Tran and P. Blaha, Accurate band gaps of semiconductors and insulators with a semilocal exchange-correlation potential, Phys. Rev. Lett., 2009, 102, 226401.

[39] G. K. H. Madsen and D. J. Singh, BoltzTraP. A code for calculating band-structure dependent quantities, Comput. Phys. Commun., 2006, 175, 67–71.

[40] Al-Muhimeed, T. I., Shafique, A., AlObaid, A. A., Morsi, M., Nazir, G., AL-Anazy, M. M., & Mahmood, Q. (2021). New lead-free double perovskites X2GeI6 (X= K, Rb, Cs) for solar cells, and renewable energy as an alternate of hybrid perovskites. International Journal of Energy Research, 45(13), 19645-19652

[41] V. M. Goldschmidt, Die Gesetze der Krystallochemie, Naturwissenschaften, 1926, 14, 477–485.

[42] A. Zunger, Practical doping principles, Appl. Phys. Lett., 2003, 83, 57–59.

[43] V. I. Anisimov, J. Zaanen and O. K. Andersen, Band theory and Mott insulators: Hubbard U instead of Stoner I, Phys. Rev. B, 1991, 44, 943–954

[44] Mir, S. A., & Gupta, D. C. (2020). Systematic investigation of the magneto-electronic structure and optical properties of new halide double perovskites Cs 2 NaMCl 6 (M= Mn, Co and Ni) by spin polarized calculations. RSC advances, 10(44), 26277-26287

[45] Rached, H., Bendaoudia, S., & Rached, D. J. M. C. (2017). Investigation of Iron-based double perovskite oxides on the magnetic phase stability, mechanical, electronic and optical properties via first-principles calculation. Materials Chemistry and Physics, 193, 453-469.

[46] Fatmi, M., Bouferrache, K., Ghebouli, M. A., Ghebouli, B., Alanazi, F. K., Albaqami, M. D., ... & Benali, A. (2025). High performance double perovskites of Cs2InAgBr6 and Cs2InAgCl6 structural electronic optical and thermoelectric properties for next-generation photovoltaics. Scientific Reports, 15(1), 20851.

[47] Kanamori, J. (1959). Superexchange interaction and symmetry properties of electron orbitals. Journal of Physics and Chemistry of Solids, 10(2-3), 87-98.

[48] Singh, U., Klarbring, J., Abrikosov, I. A., & Simak, S. I. (2023). Exploring magnetism of lead-free halide double perovskites: A high-throughput first-principles study. Physical Review Materials, 7(11), 114404.